J4.4 ESTIMATION OF SURFACE WINDS FROM SAR USING A PROJECTION ALGORITHM

Chris Wackerman
General Dynamics Advanced Information Systems, Ypsilanti Michigan USA

William G. Pichel, Xiaofeng Li,Pablo Clemente-Colòn
National Oceanic and Atmospheric Administration, NESDIS, Camp Springs MD USA

1. INTRODUCTION

As part of the NOAA/NESDIS Alaska SAR Demonstration Project (Pichel and Clemente-Colon, 2000), a multi-year demonstration of the production and use of RADARSAT SAR HH polarization imagery to generate products in a pre-operational environment, a wind product is created that automatically generates wind vectors over the coastal ocean. Two methods are used. One uses wind directions from atmospheric models that are run over the same region and close in time to the SAR image collection. These directions are then combined with the radar cross section from the SAR imagery to generate wind speed using a scatterometer model for VV imagery, and an empirically derived correction to the VV model for HH imagery, to generate the relationship between radar cross section and wind speed (Monaldo et al., 2001). The second method estimates the wind direction from the SAR imagery itself using large-scale features that are aligned with the local wind, such as wind rows, elongated convective cells, or surfactant streaks, then combines this direction with the radar cross section of the imagery to generate wind speed. The currently implemented algorithm for estimating wind direction from the SAR imagery is based on a spectral approach that uses the Fourier transform of image subsets to automatically determine directions of maximal spectral energy, then assumes that these directions correspond to 90° from the wind direction (Wackerman et al., 1996; Fetterer et al., 1998). This direction is then combined with the image radar cross section to generate wind speed using the same scatterometer model for VV and a semi-analytical two-scale model to derive the HH relationship between radar cross section and wind speed (Wackerman et al., 2002). The directions estimated from the SAR imagery have an inherent 180° ambiguity, since from a static image one can at most estimate the line along which the wind is blowing, but not the direction along that line.

One significant problem with estimating wind directions from SAR imagery is that there may not always be features in the image that the algorithm can use to estimate directions. Convective cells, wind rows, and surfactant streaks depend on there being other processes going on (such as turbulence or very little mixing of the near-surface ocean layer) rather than simply the existence of a wind field. The spectral approach that is currently implemented has no means of determining when a wind direction is able to be estimated from a region of the SAR image, and thus will often generate erroneous directions over featureless regions of the ocean surface. Therefore a study was initiated to develop a new approach for estimating wind directions, referred to here as the projection method, that would be able to recognize when no robust estimate of direction was able to be extracted from the imagery.

Corresponding author address: Chris Wackerman, General Dynamics AIS, P.O. Box 990, Ypsilanti MI 48197 USA; email; chris.wackerman@gd-ais.com

2. BACKGROUND

Satellite-based Synthetic Aperture Radar (SAR) sensors provide high resolution (12 to 100 meters) images of the earth's surface day or night and during most weather because they are active sensors operating in the microwave wavelengths (usually 3 to 20 centimeters). This makes them a potentially highly useful device for monitoring the earth, so much research has been done to determine the range of geophysical parameters that can be accurately estimated from SAR images. In particular, extracting environmental information from SAR images over the ocean has been an area of research for many years, and multiple approaches have been developed for characterizing a range of ocean parameters such as waves, winds, surf and currents. The work in this paper focuses on the use of SAR images to estimate wind vectors over the ocean and in coastal waters, and in particular to develop an operational and automated approach. If proved reliable, SAR images may be the only way to provide high spatial resolution wind vectors in coastal regions.

Almost all of these approaches to extract environmentally information from SAR images over the ocean are based on a standard theory for how a SAR images the ocean. This theory, often referred to as Bragg scattering (see Wright (1968) and Valenzuela (1978)) assumes that the variations in the SAR image brightness (or intensity) are proportional to the amplitude of ocean surface waves that are resonance to

the electromagnetic wavelength of the SAR sensor. These resonant ocean waves will have a wavenumber k_B (where $k = 2\pi/\lambda$ and λ is the wave length of the wave) such that $k_B = 2k_{EM}\sin[\theta]$ where k_{EM} is the wavenumber of the electromagnetic wavelength and θ is the incidence angle of the sensor. In addition, these resonant waves need to be propagating either directly toward or away from the sensor. Thus the SAR is only observing very small-scale waves that are propagating in very specific directions. However, these small-scale waves are highly responsive to the local wind. As the local wind speed increases the amplitudes of these waves increase and thus the SAR image brightness increases. This phenomena forms the backbone of wind retrieval from SAR since it implies that the mean SAR image brightness (or radar cross section (RCS) as it is referred to when the image is absolutely calibrated) can be related to the local wind speed and direction. Note that wind direction (relative to the direction the sensor is looking) is very important because the amplitude of the small-scale waves will change significantly according to their propagation direction with respect to the local wind. This means the SAR image RCS will also change as the SAR look direction changes even though the wind speed stays constant since the RCS is proportional to the amplitude of the waves it observes.

Much work has been done to determine how to estimate wind vectors from SAR imagery based on this theory. The general approach is shown in Figure 1. It assumes a model that predicts the RCS given wind speed and direction. The procedure is to estimate the local RCS from the SAR image, estimate wind direction either from the SAR image or from some other source (most often from satellite-based scatterometers or from atmospheric models) then find the wind speed that reproduces the observed RCS.

What differentiates the various approaches are the RCS model used and the manner to estimate wind direction. For the European ERS-1/2 SAR sensors, which operate in VV polarization, the RCS model comes from validated scatterometer models (Vachon and Dobson (1996); Wackerman et al. (1996); Fetterer et al. (1998); Lehner et al. (1998); Lehner et al. (2000)). For the Canadian RADARSAT-1 SAR sensor, which operates in HH polarization, no such validated models exist so two approaches have been tried. The first is to derive an empirical modification to the VV models to convert them to HH polarization (Horstmann et al. (2000a); Horstmann et al. (2000b); Thompson and Beal (2000); Vachon and Dobson (2000); Horstmann et al. (2002); Monaldo et al. (2001)). The second approach is to derive analytical models directly for HH polarization (Wackerman et al. (2002)).

Various approaches have also been developed for estimating the wind direction. One class of approaches estimates wind direction from the SAR image itself by noting that there are features in the imagery that tend to be aligned with the local wind. These can be wind rows, elongated convective cells, or surfactants on the ocean surface. These directions can be estimated in the spectral domain via Fourier transforms (Gerling (1986); Vachon and Dobson (1996); Wackerman et al. (1996); Fetterer et al. (1998); Lehner et al., (1998); Horstmann et al. (2000a); Horstmann et al. (2000b); Vachon and Dobson (2000)) or in the image domain via gradient estimators (Horstmann et al., 2002) or wavelet analysis (Du et al. (2002); Fichaux and Ranchin (2002)). The advantage of this class of approaches is that they generate the full wind vector solely from the SAR image without reference to any other data. The disadvantages are that the resulting wind directions have a 180° ambiguity (since from a single SAR image the feature alignment is ambiguous with respect to ±180°) and the features that are being used may not

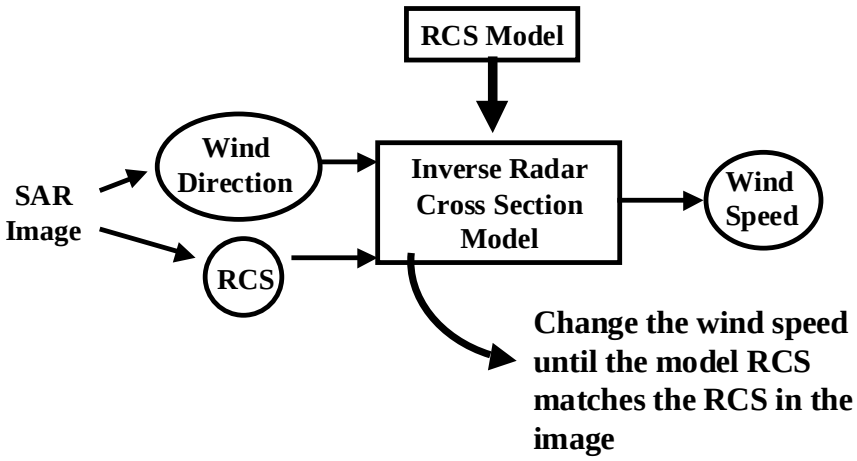

Figure 1: General approach to wind vector estimation using a SAR image.

always be present in the SAR image or aligned with the wind. The second class of approaches utilize either simultaneous satellite-based scatterometer observations or atmospheric models to derive wind directions (Thompson and Beal (2000); Monaldo (2000); Monaldo et al. (2002)). This class of approaches has the advantage that a wind direction will always be available since it is derived separately from the SAR image. The disadvantage, particularly in the use of atmospheric models, is that the directions might not correspond accurately enough to the SAR image data.

Table 1 gives a summary of performance for these algorithms drawn from a sample of the published literature. Shown in Table 1 is the reference for the results and the sensor used (ERS = the ERS sensor, RAD = the RADARSAT sensor) with the number of images that went into the error estimation (although the Vachon and Dobson (2000) results are for the number of comparisons since the number of images was not described). Next is shown the root-mean-squared error (RMSE) for estimating wind direction from the SAR image. Note that all but the two indicated results used spectral approaches for estimating wind direction. Finally, the RMSE for wind speed is shown where three different wind directions are used. In the first column the direction derived from the SAR image is used, in the next column directions from a satellite-based scatterometer are used, in the last column directions from an atmospheric model are used. For the atmospheric models, the model name is indicated below the error. The performance of the various algorithms are very similar, and to derive a general sense of performance, the RMSE values are averaged over the different sources and shown on the bottom. General wind direction RMSE is 31 degrees and wind speed RMSE is around 2.2 m/s.

Source	**Sensor/# of images**	**Dir. RMSE**	**Speed RMSE (SAR dir.)**	**Speed RMSE (Scat. dir.)**	**Speed RMSE (model dir.)**
Wackerman et al. 1996	ERS/9	19°	1.2 m/s		
Fetterer et al. 1998	ERS/61	37°	2.0 m/s		
Vachon and Dobson 2000	ERS/65[1]	40°	1.9 m/s		
Vachon and Dobson 2000	RAD/77[1]	40°	2.4 m/s		
Horstmann et al. 2000a	RAD/4			2.7 m/s	
Horstmann et al. 2000a	RAD/9				2.9 m/s (HIRLAM)
Fichaux and Rachin 2002 (direction via wavlets)	ERS/1	16°			
Horstmann et al. 2002 (direction via gradient)	RAD/20	22°	3.5 m/s		
Monaldo et al. 2001	RAD/2862				2.0 m/s (NOGAPS)
This paper (directions via projection method)	RAD/213[1]	41°	2.2 m/s		
Average Value		31°	2.2 m/s	2.7 m/s	2.5 m/s

[1] Number of comparisons, not number of images.

Table 1: Summary of wind vector estimation performance from various published papers.

3. PROJECTION METHOD FOR WIND DIRECTION ESTIMATION

There are a number of problems with the existing spectral based approach for estimating wind direction directly from the SAR image. One problem is that there may not be a feature aligned with the wind in all parts of the image, and it would be ideal if the algorithm could recognize this and not report a wind direction for image regions that do not have sufficient signatures. A second problem is with the accuracy of estimating directions from low frequency information in the spectrum. Because the image features aligned with the wind often have large scales, their spectral energy is clustered near to the origin. Estimating the direction of elongation of that energy (the dominant method that spectral approaches use to estimate wind direction) can often therefore only be done in increments of 45 degrees because of the sampling of the spectral energy that close to the origin.

To try and address these problems, we have developed a new approach to estimating wind direction directly from the imagery based on projections of the image values at various angles. By the Projection-Slice theorem, the projection of an image is equal to the Fourier transform of a radial cut through the Fourier transform of the image. Thus by working with projections in the image space, we can sample directions in the spectrum as finely as we want, without

being hampered by the spectral spacing close to the origin. This solves the second problem mentioned above. To address the first problem, we have implemented a test on the contrast or variations of the projections in order to determine when a feature of sufficient "strength" is present in the image to use for a wind direction estimate. If such a feature is not present, we can then move on to a different portion of the image and not generate a wind vector over such "blank" regions. Thus we only generate wind vectors over portions of the image that contain adequate features.

It should be noted that mathematically we haven't changed much from the previous spectral approach. Estimating the contrast or variation of the projection of an image is mathematically equivalent to finding the spectral energy or extent along a radial line of the image spectrum. Thus we would have achieved the same algorithm by simply re-sampling the image spectrum along radial lines and looking for the lines of largest spectral extent or spectral energy. However, it is computationally easier to work with image projections; a look-up table can be generated initially to determine which image subset samples get added into which projections and then each set of projections can be calculated with just a look-up and summing operation. Also, by working in the image domain, we can be somewhat more intuitive in how we estimate feature "strength" for thresholding.

The new algorithm proceeds as follows. The user determines a window size that will be moved through the image, and for each placement of the window one wind vector will be estimated. The window size should be driven by the scales of the features that are going to be used to estimate wind direction. For wind rows, these are typical from 3 to 10 km, so usually the window should not be much smaller than 10 km. For the results in this paper, a 24 km window was used and the window was shifted every 16 km to generate a new wind vector estimate, thus there is some overlap of image samples used to create successive wind vectors. For a given window placement, the projection of the image samples within the window along a direction are generated for directions from -90° to +90°. That is, for each direction a one-dimensional function is generated by stepping through the middle of the window in the specific direction, and at each image sample along that direction averaging all of the image samples that are in the orthogonal direction. For the results in this paper a projection was calculated every 1°, however in the results below (particularly Fig. 3) it can be seen that one could use a coarser angular sampling of the projections as long as the peaks of the feature contrasts (as defined below) can be resolved. This projection is then flattened to remove linear trends in the function.

As mentioned above, the projections are generated by creating a look-up table initially that maps the image samples to the projection lines that image sample need to be summed into. This look-up table is the same for every placement of the window, so each set of projections from a given window placement is generated simply by a look-up and sum operation.

Fig. 2 shows an example where the right image displays the SAR image values within a local window, and the left image displays the resulting projections for the full range of angles, with a different projection at each line. The algorithm needs to locate the angle of the projection that contains the largest fluctuations. This will be the projection that is orthogonal to the "crests" of the wind row features observed in the SAR image subset. In the projection image, one can see that this projection angle occurs at approximately +45º where very bright and dark "blobs" can be seen in the projection. A number of metrics could be used to estimate fluctuations in the projections. We have implemented the contrast (standard deviation divided by the mean) calculated for the whole projection line, however other groups use the gradient (Horstmann et al., 2002) over various spatial scales (note that the one-dimensional gradient along a projection line is equivalent to a two-dimensional gradient in the direction of the projection line) and one could also use the spectral content of the projection over some spectral window. Note that this last approach gets us back to the original spectral algorithm, when the spectrum energy only within an annulus is used. We have implemented the contrast mainly because it is easy to calculate, and we have not yet found any compelling evidence that one metric is significantly better than another.

Fig. 3 shows the resulting contrast plot generated from the projections shown in Fig. 2. If the maximum contrast value is above some threshold, then 90° from this direction is the estimated wind direction for this window. For the results in this paper, the contrast threshold was set to 0.04 based on manual analysis of the obvious visual features in the imagery. Note however that although this metric is invariant to scale factors, it may depend on the processor used since the contrast of a feature will change whether the image was saved as 8 bits, 16 bits, in log values, etc. Thresholding the contrast of the projection allows the algorithm to not generate a wind direction for image regions where there are no features with sufficient modulation to be used for wind direction estimation.

Fig. 4 shows the results of varying the contrast threshold for a SAR image. The top left image shows direction results (indicated as white lines on the image)

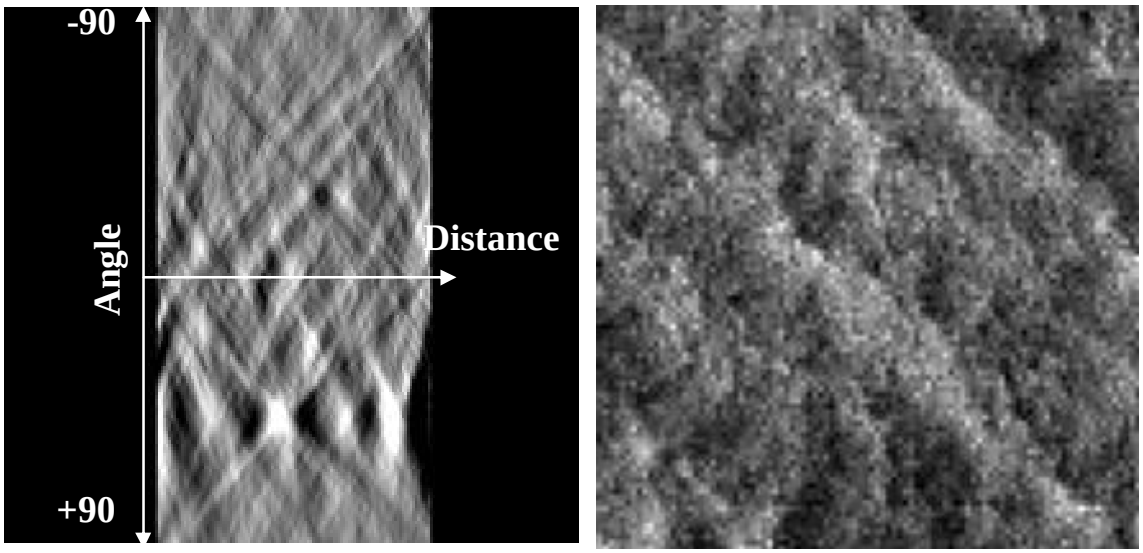

Figure 2: Right image shows a subset of a SAR image with wind row features. Left image shows the resulting projections from the image subset.

when no threshold is applied. The top right and bottom images show results for thresholds of 0.03 and 0.06 respectively. Note that as the threshold increases, we filter out all but the highest contrast features to use, and automatically eliminate the low contrast regions which were generating erroneous directions under the spectral approaches. As mentioned above, we chose 0.04 as the threshold.

The next step in the algorithm is to eliminate outliers; wind directions that are significantly different than their neighbors. This is done by calculating, for each output wind vector, the total number of wind vectors in a 5 x 5 neighborhood around the output wind vector, and the number of vectors in the neighborhood that have the same direction (less than 30º absolute difference). If there are less than 7 neighbors, we leave the vector alone since there is not enough neighbors to make a determination as to whether the direction is an outlier. If there are at least 7 vectors in the neighborhood but

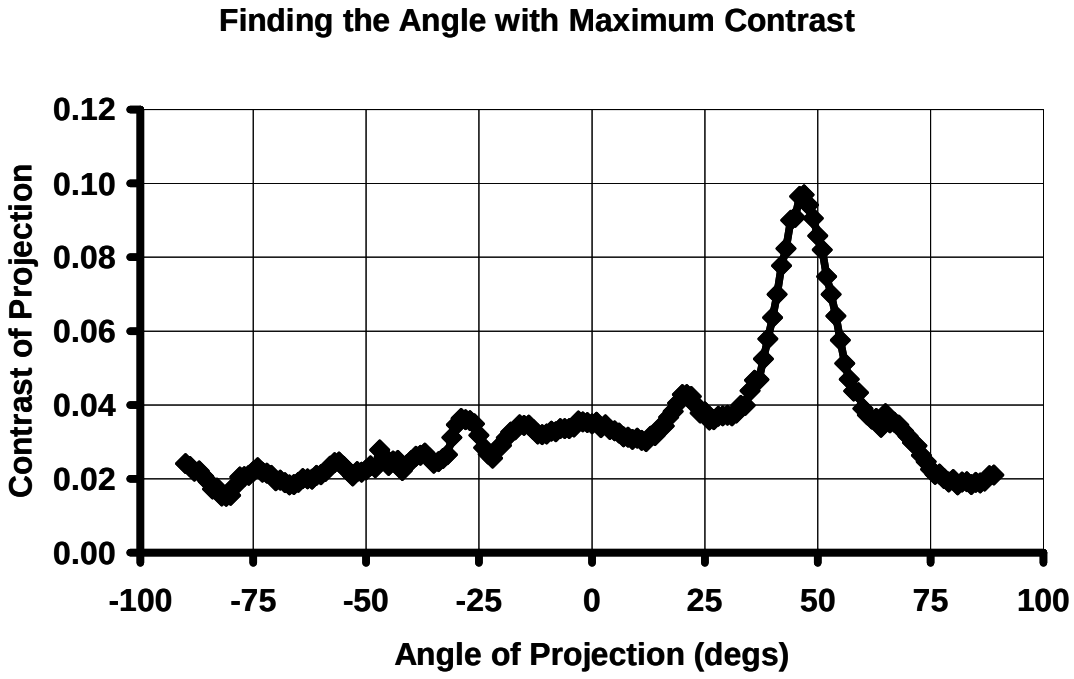

Figure 3: A plot of contrast versus projection angle for the projections shown in Fig. 1. The global maximum at an angle of approximately +45º is the estimated wind direction.

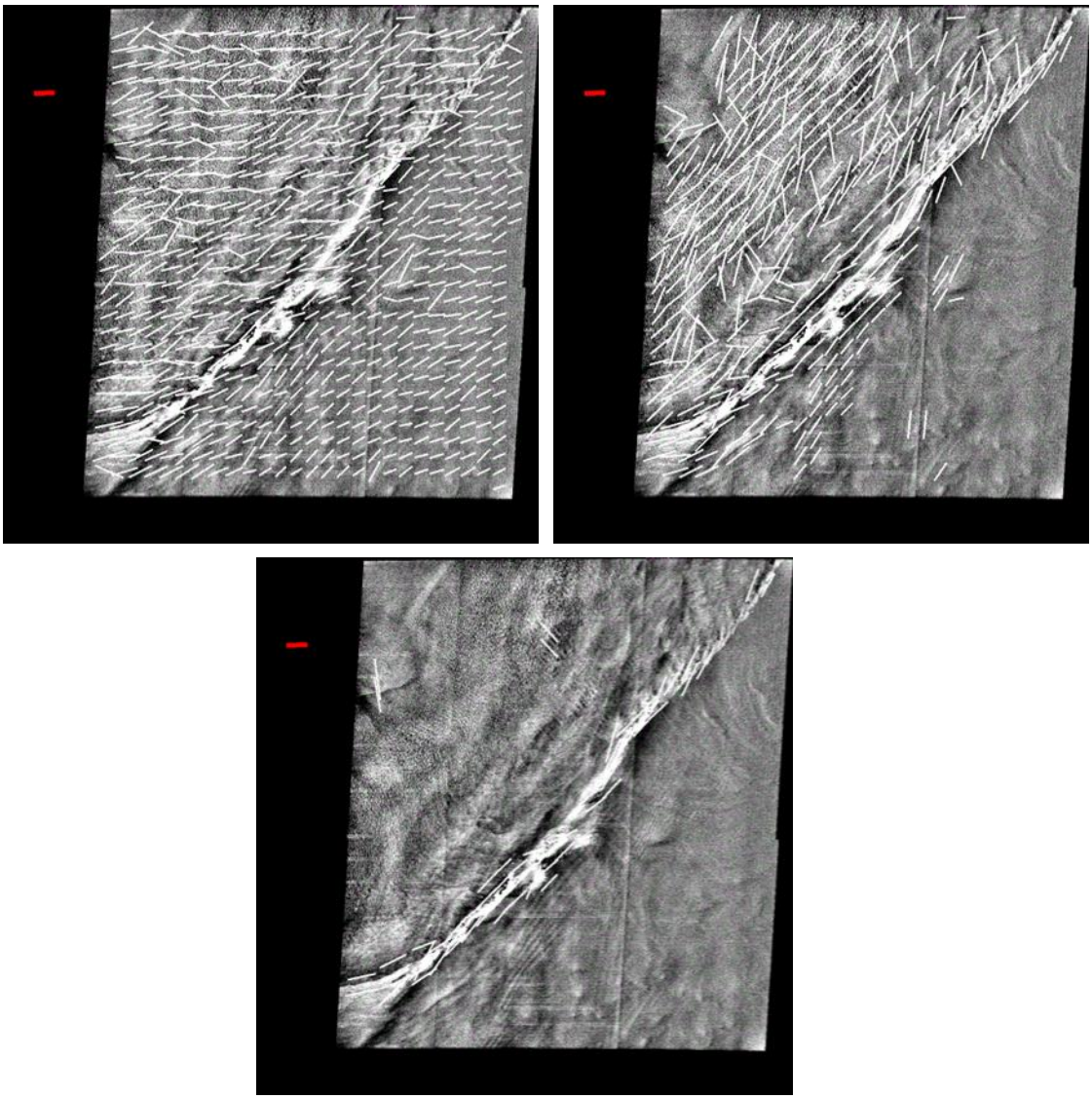

Figure 4: Examples of using the threshold on projection contrast to remove image regions with no strong features. Top left image shows estimated wind directions (white lines) with no threshold, top right image has a threshold of 0.03, and the bottom image 0.06. The red line on the left shows the buoy derived wind directions. Image was collected March 29 2000 at 10:51:14. ©Canadian Space Agency 2000

only 3 or less neighbors have the same direction, this vector is considered an outlyer and removed.

The final step in estimating wind vectors is to apply a median-like operation to the wind vectors to smooth the vector field. This is done by replacing the wind vector in the middle of a local box by the vector within the box that minimizes the norm of the difference between that vector and all of the others within some local region (we use 11 x 11 vectors). Note that this approach has the advantage of only using wind vectors that have been estimated from the image (i.e. we do not average vectors such that a resulting vector was never seen anywhere in the image), and of preserving wind fronts in the final wind vector map. The amount of smoothing is controlled by the number of times the median filter is iteratively applied. We use only a single iteration to provide the smallest amount of smoothing.

To generate a uniform wind field, wind directions are generate over image locations for which we did not have an appropriate feature for estimating the direction directly by interpolation from surrounding directions. The interpolation is done as a weighted linear combination where the weights are 1/(distance**2) and we make sure that we use the nearest locations in all

four quadrants. The wind speed then comes from using this direction with the local RCS values. In the images that follow, thick white line represent wind vectors for which the directions came from the image, thin lines represent wind vector for which the directions came from interpolation.

4. PROJECTION ALGORITHM PERFORMANCE ON RADARSAT IMAGERY

To determine how well the projection approach estimated the actual wind direction we used a series of RADARSAT SAR images collected off the east coast of the United States for which there was buoy wind information generated approximately simultaneously with the image acquisition and located spatially within the SAR image. The SAR imagery was processed at the Alaska Satellite Facility and represented 100 m resolution imagery with 50 m sample spacing. The buoy winds were converted to 10 m winds to make them consistent with the radar cross section models being used to estimate wind speed. The buoy information was compared to wind vectors estimated from the SAR image derived close to where the buoy was located. We eliminated any comparisons that occurred at incidence angles less than 25° due to possible calibration errors in the processed image, any comparisons for which the SAR-derived vector was more than 48 km away from the buoy location, and any comparisons for which the buoy wind speed values were less than 5 m/s, since for these locations there may be no significant radar cross section response from the ocean surface. Note that although 48 km is somewhat far from the *in situ* observations for comparison, it was used since that was twice the size of our local image window.

These constraints resulted in a total of 213 comparisons between buoy observations and wind vectors estimated from the SAR imagery. A plot of SAR-derived wind direction vs. buoy wind direction is shown in Fig. 5. Due to the 180° ambiguity in the SAR-derived directions, a value of 180 was added or subtracted from the SAR-derived direction to get it within ±90° from the buoy direction. In Fig. 5 the solid black line represents a perfect answer, i.e. the SAR-derived direction equals the buoy direction, and the dashed lines are ±90° from the solid line which represents the region of possible SAR-derived values. The final root-mean-squared error (RMSE) is 41° (mean error of 7°). Note that if we were to randomly assign a direction uniformly in the range of [-90°, +90°] we would expect a RMSE of 52°, which looks like we are only slight better than a random guess. However, an examination of the errors in Fig. 5 shows that they are not uniformly distributed, but rather tend to cluster

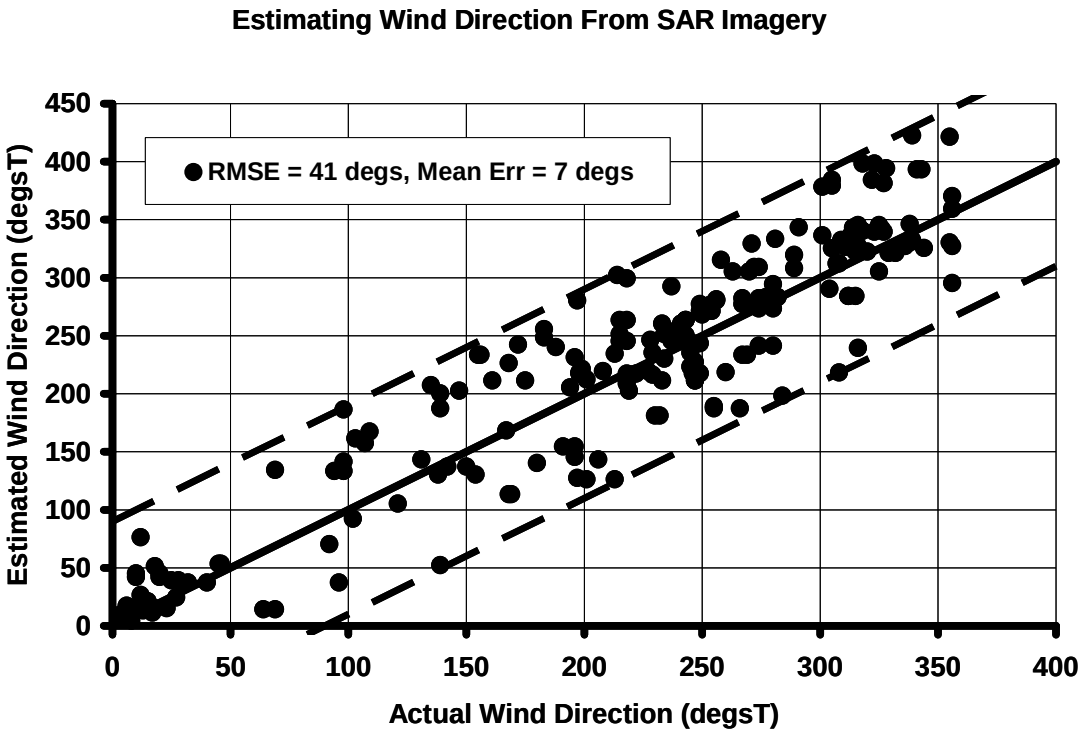

Figure 5. Scatterplot of actual wind direction from buoy observations vs. SAR-derived wind directions. The total RMSE is 41º, the mean error is 7º. If we remove seven images that have features not aligned with the wind, the RMSE becomes 39º.

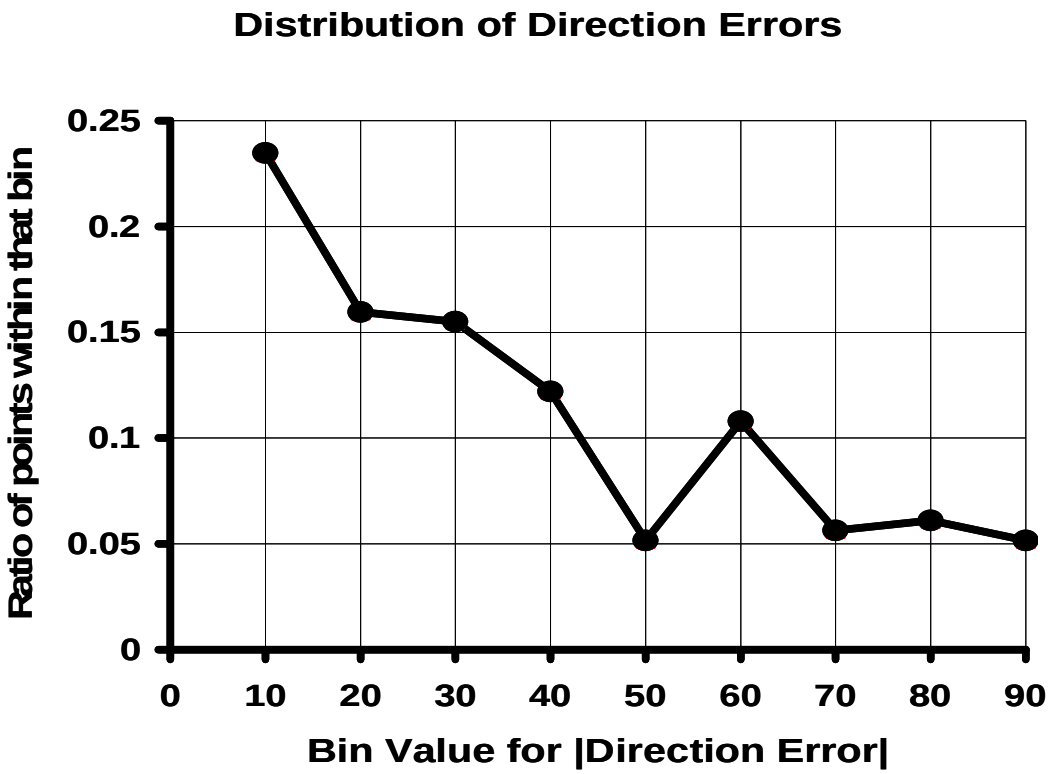

Figure 6: histogram of the absolute value of the direction error. X-axis is the bin value for the error, y-axis is the ratio of points that fall into that bin. Note that 52% of the samples have errors less than 30º.

around the "perfect" line. This is shown quantitatively in Fig. 6, where a histogram of the absolute value of the direction error is plotted. The x-axis of Fig. 6 is the top value of the error bin for the histogram. Thus the first point represents errors of 10° or less, the second points represents errors between 20° and 10°, etc. Fig. 6 indicates that 54% of all of samples have an absolute direction error that is less than 30°. Note that if we were uniformly guessing a direction, the histogram in Fig. 6 would be a flat line around 0.1. The results in Figs. 5 and 6 were generated automatically; the algorithm was run with no user interaction or modification of the resulting directions.

Fig. 5 shows that there are a number of comparisons for which the estimated wind direction is as worse as it can get; i.e. 90° from the true direction. In fact, Fig. 5 shows a number of isolated points that are almost right on the ±90°. From manually examining these images we have found that typically these are caused by there being a feature in the image that has high contrast but is not aligned with the local wind. Usually these are lee waves near to a coastline or island, convective cells caused by large downdrafts, or surfactant streaks being oriented by a current instead of the local wind. This is one of the significant remaining problem with automated extraction of wind directions from SAR is being able to automatically classify the image features (i.e. into convective cell, current front, wind row, wind front, surfactants, etc.) so that we can eliminate those high contrast features that are not connected with the local wind (such as lee waves) or which need to be treated differently then just aligning with the direction of highest contrast (such as convective cells).

We will note however that there were seven images for which either the algorithm was keying on a feature not aligned with the wind (lee wave, convective cell, or current front) or the buoy data just did not appear to align with the image information. If we removed these from consideration, we lost ten of the comparisons out of 213, but this decreased the RMSE to 39º. Thus these seven images had a large impact on the error. However, since we do not have an automated way to estimate these types of features, we have not included this error into the operational estimate.

Fig. 7 shows a comparison of estimated wind speed versus buoy wind speed for this data set. The black dots used the wind direction as derived from the SAR

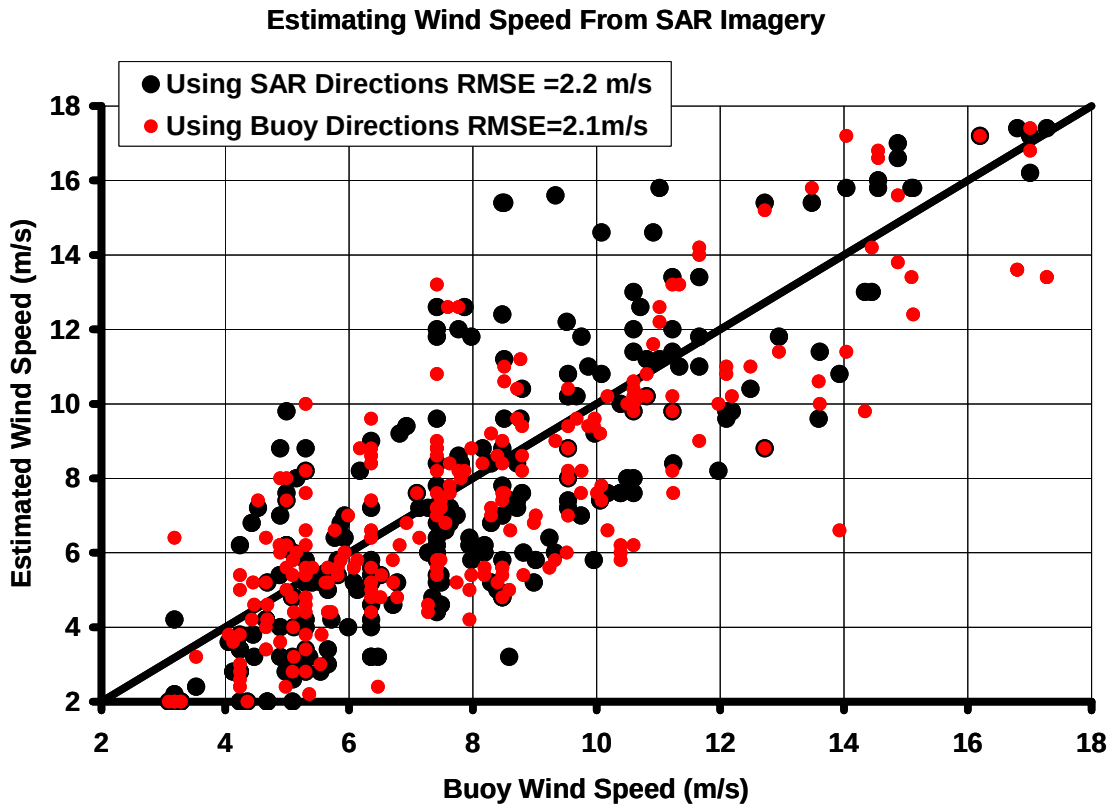

Figure 7: Estimated wind speed from the SAR imagery vs. buoy wind speed. Black dots are using SAR-derived directions and have a RMSE of 2.2 m/s (mean error = -.28 m/s). Red dots are using buoy directions and have a RMSE of 2.1 m/s (mean error =-.59 m/s).

image and the radar cross section model in (Wackerman et al., 2002). The RMSE is 2.2 m/s (mean error = -0.28 m/s). The red dots used the buoy wind directions and the same radar cross section model; the RMSE is 2.1 m/s (mean error = -0.59 m/s). Note that there is not much difference between using the SAR-derived directions or the buoy directions, other than a cluster of 5 points in the upper, center, indicating that error in wind direction are not the dominant cause of the scatter in wind speed estimation.

In summary, the algorithm has been tested operationally on RADARSAT imagery that contained *in situ* buoy-derived wind speed and direction information. The algorithm was run automatically without any user inputs. The wind direction root-mean-squared error is 41º, with a mean error of 7º. The wind speed root-mean-squared error is 2.2 m/s, with a mean error of -0.28 m/s. If we remove seven images with "bad" features, the RMSE for direction drops to 39º.

5. ACKNOWLEDGEMENTS

This study was supported and monitored by the Office of Research and Applications of the National Oceanic and Atmospheric Administration (NOAA) under ONR Contract N00014-00-D-0114.

The views, opinions, and findings contained in this report are those of the authors and should not be construed as an official National Oceanic and Atmospheric Administration of U.S. Government position, policy or decision.

6. REFERENCES

Du, Y., P. Vachon, J. Wolf, 2002: Wind direction estimation from SAR images of the ocean using wavelet analysis, *Can. J. Remote Sens.*, **28**, 498-509

Fetterer, F., D. Gineris, C. Wackerman, 1998: Validating a scatterometer wind algorithm for ERS-1 SAR. *IEEE Trans. Geosc. Remote Sens.*, **36**, 479-492

Fichaux, N., T. Rachin, 2002: Combined extraction of high spatial resolution wind speed and direction from SAR images: a new approach using wavelet transform, *Can. J. Remote Sens.*, **28**, 510-516

Gerling, T.W. 1986: Structure of the surface wind field from SEASAT SAR, *J. Geophys. Res*., **91**, 2308-2320

Horstmann, J., W. Koch, S. Lehner, R. Tonboe, 2000a: Wind retrieval over the ocean using synthetic aperture radar with C-band HH polarization. . *IEEE Trans. Geosc. Remote Sens.*, **38**, 2122-2131

Horstmann, J., S. Lehner, W. Koch, R. Tonboe, 2000b: Computation of wind vectors over the ocean using spaceborne synthetic aperture radar, *The John Hopkins Univ. Tech. Dig.*, **21**, 100-107.

Horstmann, J., W. Koch, S. Lehner, R. Toeboe, 2002: Ocean winds from RADARSAT-1 ScanSAR, *Can. J. Remote Sens.*, **28**, 524-533

Lehner, S., J. Horstmann, W. Koch, W. Rosenthal, 1998: Mesoscale wind measurements using recalibrated ERS SAR images, *J. Geophys. Res*., **103**,7847-7856

Lehner, S., J. Schulz-Stellenfleth, B. Schattler, H. Breit, J. Horstmann, 2000: Wind and wave measurements using complex ERS-2 SAR wave mode data, *IEEE Trans. Geosc. Remote Sens.*, **38**, 2246-2257

Monaldo, F., 2000: The Alaska SAR demonstration and near-real-time synthetic aperture winds, *The John Hopkins Univ. Tech. Dig*., **21**, 75-79

Monaldo, F., D.R. Thompson, R.C. Beal, W.G. Pichel, P. Clemente-Colon, 2001: Comparison of SAR-derived wind speed with model predictions and ocean buoy measurements, *IEEE Trans. Geosc. Remote Sens.*, **39**, 2587-2600

Pichel, W.G., P. Clemente-Colon, 2000: NOAA coastwatch SAR applications and demontrations, *The John Hopkins Univ. Tech. Dig.*, **21**, 49-57

Thompson, D.R., R.C. Beal, 2000: Mapping high-resolution wind fields using synthetic aperture radar, *The John Hopkins Univ. Tech. Dig.*, **21**, 58-67

Vachon, P., F.W. Dobson, 1996: Validation of wind vector retrieval from ERS-1 SAR images over the ocean, *Global Atmos. Ocean Syst.*, 177-187

Vachon, P., F.W. Dobson, 2000: Wind retrieval from RADARSAT SAR images: selection of a suitable C-band HH polarization wind retrieval model, *Can. J. Remote Sens.*, **26**, 306-313

Valenzuela, G.R., 1978: Theories for the interaction of electromagnetic and oceanic waves – a review, *Boundary-Layer Meteorology*, **13**, 61-85

Wackerman, C., C.L. Rufenach, R.A. Shuchman, J.A. Johannessen, K.L. Davidson, 1996: Wind vector retrieval using ERS-1 synthetic aperture radar imagery, *IEEE Trans. Geosc. Remote Sens.*, **34**, 1343-1352

Wackerman, C., P. Clemente-Colon, W. Pichel, X. Li, 2002: A two-scale model to predict C-band VV and HH normalized radar cross section values over the ocean, *Can. J. Remote Sens.*, **28**, 367-384

Wright, J.W., 1968: A new model for sea clutter, *IEEE Trans. Antennas and Propagation.*, **AP-16**, 217-223